NANO LETTERS

Letter

pubs.acs.org/NanoLett

Nanoimprint-Transfer-Patterned Solids Enhance Light Absorption in Colloidal Quantum Dot Solar Cells

Younghoon Kim, Kristopher Bicanic, Hairen Tan, Olivier Ouellette, Brandon R. Sutherland, F. Pelayo García de Arquer, Jea Woong Jo, Mengxia Liu, Bin Sun, Min Liu, Sjoerd Hoogland, and Edward H. Sargent*

Department of Electrical and Computer Engineering, University of Toronto, 10 King's College Road, Toronto, Ontario M5S 3G4, Canada

Supporting Information

ABSTRACT: Colloidal quantum dot (CQD) materials are of interest in thin-film solar cells due to their size-tunable bandgap and low-cost solution-processing. However, CQD solar cells suffer from inefficient charge extraction over the film thicknesses required for complete absorption of solar light. Here we show a new strategy to enhance light absorption in CQD solar cells by nanostructuring the CQD film itself at the back interface. We use two-dimensional finite-difference time-domain (FDTD) simulations to study quantitatively the light absorption enhancement in nanostructured back interfaces in CQD solar cells. We implement this experimentally by demonstrating a nanoimprint-transfer-patterning (NTP) process for the fabrication of nanostructured CQD solids with highly ordered patterns. We show that this approach enables a boost in the power conversion efficiency in CQD solar cells primarily due to an increase in short-circuit current density as a result of enhanced absorption through light-trapping.

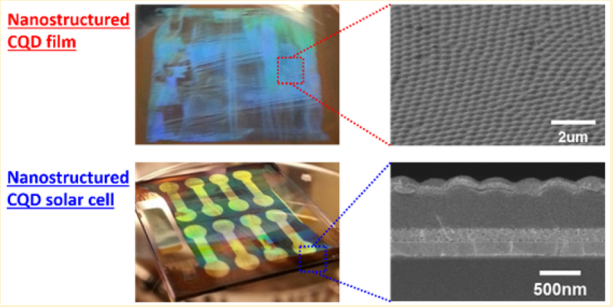

KEYWORDS: *Colloidal quantum dots, photovoltaics, nanostructured quantum dot solids, light trapping*

Colloidal quantum dot (CQD) solids are promising photoactive materials for solution-processed thin-film optoelectronic devices such as photovoltaics[1−4] and light-emitting diodes (LEDs)[5−8] due to their size-tunable bandgap, low-cost processing, and their potential for large-scale fabrication. CQD photovoltaic performance has steadily improved over the past few years as a result of enhanced CQD passivation and improved device architectures.[9−14] Recently, the certified power conversion efficiency (PCE) of CQD solar cells has reached 11.3%.[15] This was accomplished using PbI_2-passivated CQD solids with flat energy landscapes achieved by preserving CQD monodispersity in final films.[16]

Unfortunately, CQD photovoltaic devices suffer inefficient charge extraction when made thick enough to provide complete optical absorption:[17−19] their charge diffusion length is less than the longest above-gap optical absorption length. Photogenerated charges recombine before being extracted at the electrodes, resulting in a significant amount of wasted light.[17]

Researchers have sought to develop device architectures that overcome this absorption−extraction compromise. These include bulk heterojunctions, plasmonic nanostructures, and structured electrodes for light trapping.[10,11,20−29] Nanoimprinting and stamping techniques have been utilized to pattern the transparent conductive oxide (TCO) electrodes and have enabled the enhancement of light trapping in bottom-illuminated CQD solar cells at the front side interface between the photoactive CQD layer and the nanostructured TCO electrode.[26−30]

These approaches, which rely on the nanostructuring of bottom electrode layers, require conformal coating of each subsequent layer, including the photoactive CQDs and the TCO materials (i.e., ITO, ZnO, TiO_2, and so forth). They therefore cannot use conventional deposition processes (e.g., spin-coating) of each material in the device stack, because these processes are planarizing.[26−30] In addition, the deposition and device architecture need to be reoptimized to retain photovoltaic performance.

Back-side structuring is the most efficient way to enhance broadband light absorption in thin-film solar cells.[31,32] However, this approach has yet to be demonstrated in CQD solar cells. Achieving high-quality nanostructured CQD solids for use in back-side structured photovoltaics requires innovations in materials processing strategies.

In light of these challenges, we sought to develop a nanostructured back-mirror at the interface between the photoactive CQD layer and top metal gold electrode in the bottom-illuminated device architecture. Because of the large difference between the refractive index of CQD and gold, enhanced light trapping in the CQD film is expected from strong light scattering at the nanostructured back interface.[33,34] Direct stamping of soft

Received: December 18, 2016
Revised: February 16, 2017
Published: March 13, 2017

DOI: 10.1021/acs.nanolett.6b05241
Nano Lett. XXXX, XXX, XXX−XXX

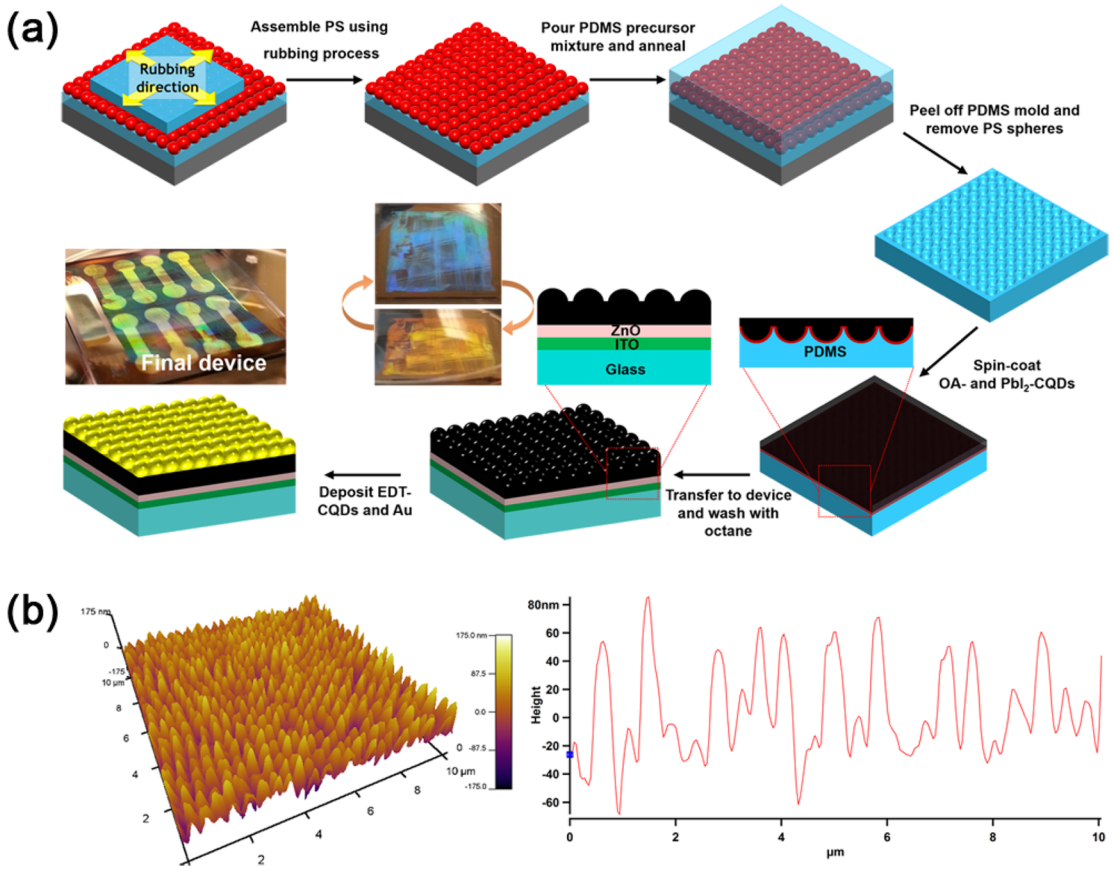

Figure 1. (a) Schematic illustration of the fabrication of patterned PDMS mold and nanostructured CQD solar cells. (b) AFM image and line profile of the nanostructured CQD film.

polymer layers has been used to fabricate a nanostructured back interface in organic photovoltaics (OPVs);[35] however, it is not be directly applicable to inorganic CQD films as they are rigid following spin-coating. Dielectric colloidal spheres have been embedded into the back interface between a CQD layer and a metal electrode to improve light absorption as optical resonators;[36] however, the performance improvement has been limited due to a loss of contact area between the CQD layer and the metal electrode.

Herein we demonstrate a new pattering process that defines CQD-only nanostructured photoactive solids with high-quality patterns. The approach does not require template incorporation into films (Figure 1). The procedure, which we termed nanoimprint-transfer-patterning (NTP), begins with off-substrate nanostructuring of CQD films; these are then transferred to a device substrate and enable formation of a nanostructured back interface in the best bottom-illuminated CQD solar cell architecture.[4,16] The approach enables a boost in PCE primarily due to increased short-circuit current density (J_{SC}) in the best CQD solar cells. This enhancement is attributed to improved light absorption via enhanced light trapping from the back interface between the nanostructured CQD layer and top gold electrode in bottom-illuminated device architectures.

A schematic showing the NTP process for the fabrication of nanostructured CQD films is illustrated in Figure 1a. First, polystyrene (PS) microspheres of diameter 500 nm were hexagonally assembled onto the cured poly(dimethylsiloxane) (PDMS) substrate using a mechanical rubbing process.[37] The PDMS precursor mixtures were poured into the PS-assembled PDMS substrate and cured at 120 °C for 2 h. The cured PDMS film was peeled from the PS-assembled PDMS substrate and soaked in acetone overnight to remove completely the remaining PS microspheres.[38] We use this as a mold to fabricate the nanostructured CQD films with round-shaped motifs (see details in Experimental Section in Supporting Information).

For nanoimprinting CQDs, oleic acid-stabilized PbS CQDs (OA-CQDs) dispersed in octane were first spin-coated onto the resulting PDMS mold, and subsequently PbI_2-passivated PbS CQDs (PbI_2-CQDs) dispersed in *n*-butylamine were spin-coated onto this layer. These OA-CQDs were used to increase the wettability of hydrophilic PbI_2-CQD solutions onto the hydrophobic PDMS mold and to transfer readily the PbI_2-CQD layer from the PDMS mold to the primary PbI_2-CQD layer. The latter had been prespin-coated onto an ITO glass substrate with a ZnO electron accepting layer (Figure S1 in the Supporting Information). After transferring completely, we removed the OA-CQDs remaining onto the PbI_2-CQD layer by washing with octane. This results in a nanostructured photoactive film with round-shaped motifs comprised exclusively of PbI_2-CQDs. To complete device fabrication, we deposited thin layers of 1,2-ethanedithiol (EDT)-treated PbS CQDs (EDT-CQDs) onto the nanostructured PbI_2-CQD film, followed by gold deposition as a top metal electrode (Figure 1a).

Figure 1b is an atomic force microscopy (AFM) showing the surface of the nanostructured photoactive layer, composed of the thick PbI_2-CQDs and thin EDT-CQDs. The results demonstrate that the NTP process enables the fabrication of nanostructured CQD-only films with round-shaped periodic motifs. The film morphologies are investigated further by optical microscopy and AFM over a range of regions of the same

DOI: 10.1021/acs.nanolett.6b05241
Nano Lett. XXXX, XXX, XXX−XXX

sample (Figure S2 in the Supporting Information). The nanostructured film has a densely, closely and uniformly packed morphology of round-shaped patterns composed of CQD solid. Scanning electron microscopy (SEM) confirmed the feature size of the rounded patterns from the cross-sectional SEM image (Figure S3 in the Supporting Information).

We leveraged our NTP process to obtain patterned CQD layers in solar cell devices. We fabricated flat control samples using the same concentration of PbI_2-CQD solutions in order to compare the optical absorption and device performance of each device at the same total thickness. In the case of the flat control, the PbI_2-CQDs corresponding to the PbI_2-CQDs coated onto the PDMS mold was spin-coated onto the precoated PbI_2-CQD layer instead of using a transferring technique and was followed by two EDT-CQD layers and gold deposition. Schematic illustrations of each device are shown in Figure 2a.

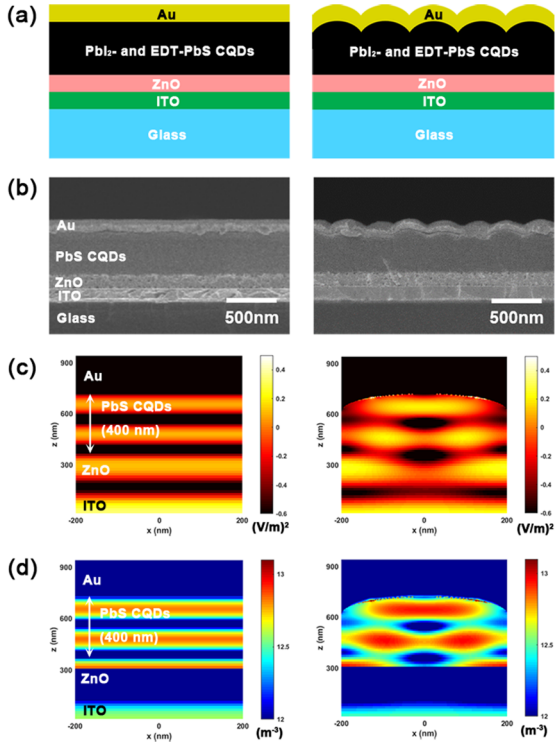

Figure 2. (a) Schematic illustration of the device cross-section. (b) Cross-sectional SEM images. (c) Color plots of the electric field intensities ($[E]^2$). (d) Color plots of the absorption power profiles per unit volume of a flat control (left) and nanostructured device (right).

Cross-sectional SEM images in Figure 2b were measured to verify that each device has the same total thickness. As a result, the nanostructured CQD layer has in fact a slightly smaller active volume. Neither pinhole nor boundary layers are seen in the nanostructured CQD layers transferred from the PDMS mold to the device.

Using knowledge of the film thickness and feature size, we used 2D finite-difference time-domain (FDTD) simulations to model light absorption in the solar cells using a normal incidence plane wave source (see details in Experimental Section in Supporting Information). These simulations used measured optical parameters for glass substrate/ITO (150 nm)/ZnO (150 nm)/PbI_2- and EDT-CQDs (420 nm)/gold (120 nm).

We calculated the electric field intensity ($[E]^2$) distribution at the exciton wavelength (λ_{exc}) = 950 nm for the flat and nanostructured devices using the FDTD simulations (Figure 2c). In the case of flat device, a standing wave was present due to interference in the photoactive layer between the incident light and the light reflected by the gold mirror. In contrast, the nanostructured device showed an overall broadband enhancement over the active region with a more concentrated field intensity at the center region of the half hemisphere and two conformal points in the flat region of the CQD layer. This enables enhanced absorption throughout the photoactive layer at the same total thickness. The power absorption profiles are also obtained using FDTD simulations (Figure 2d).

The FDTD simulations allow estimation of total absorption in each device structure with and without the top gold electrode (Figure 3a,b). The experimental total absorption is also obtained from UV−vis-IR spectroscopy measurements of each device with and without the top gold electrode (Figure 3c,d). The results obtained from the FDTD simulations agree well with measured total absorptions. Minor discrepancies can be attributed to nonideal periodicity, imperfections within the film, and feature size variation of embossed-nanostructures.[39]

In the case of no top gold electrode, the simulated absorption spectra in Figure 3a show a similar trend between flat and nanostructured devices, a result of minimal light reflection because of a small refractive index contrast between CQDs and air, compared with CQDs and gold; nevertheless, there is still a small degree of light trapping resulting in an enhancement in absorption. Each device with the top gold electrode (Figure 3b) shows a large broadband absorption improvement, a finding that agrees well with the simulated electric field and absorbed power results of Figure 2c,d.

Figure 4a presents the current density−voltage (J−V) curves of the flat and nanostructured CQD solar cell devices under simulated AM1.5 illumination. As demonstrated in FDTD simulations and optical characterization, the nanostructured CQD morphologies give rise to a notable increase of photovoltaic performance through an increase in a J_{SC}, which reaches 27.8 mA/cm^2. The open-circuit voltage (V_{OC}) and fill factor (FF) of the nanostructured device were each decreased compared to the flat control device. The histogram of device performance for both flat and pattern CQD solar cells indicates that the device results are reproducible (Figure S4 in the Supporting Information). The bilayer flat device was additionally fabricated by transferring a flat CQD layer, which was spin-coated onto the flat PDMS mold, to the target device in order to determine whether the drop in V_{OC} and FF results from the interface formed by the transferring process. However, we observed no drop in device performance from this bilayer flat device compared to the flat control (Figure S5 in the Supporting Information). Instead, we conclude that the drop in V_{OC} and FF can be attributed to the nonconformal coating of EDT-CQDs, which were spin-coated onto the nanostructured PbI_2-CQD film as a hole-transport layer (Figure S6 in the Supporting Information).[40] Overall, PCE increased from 9.8% to 10.1% because of the significant increase in J_{SC} value (from 25.0 to 27.8 mA/cm^2).

The external quantum efficiency (EQE) spectrum for each device was measured in order to investigate the origin of the enhanced light trapping effect in the nanostructured CQD devices. As seen in Figure 4b, the nanostructured solar cells have increased EQE values over the full spectral range with an expected J_{SC} of 28.9 mA/cm^2 agreeing with the measured J_{SC} (27.8 mA/cm^2) to within 5%. The EQE spectrum of the nanostructured device included a significant enhancement of

DOI: 10.1021/acs.nanolett.6b05241
Nano Lett. XXXX, XXX, XXX−XXX

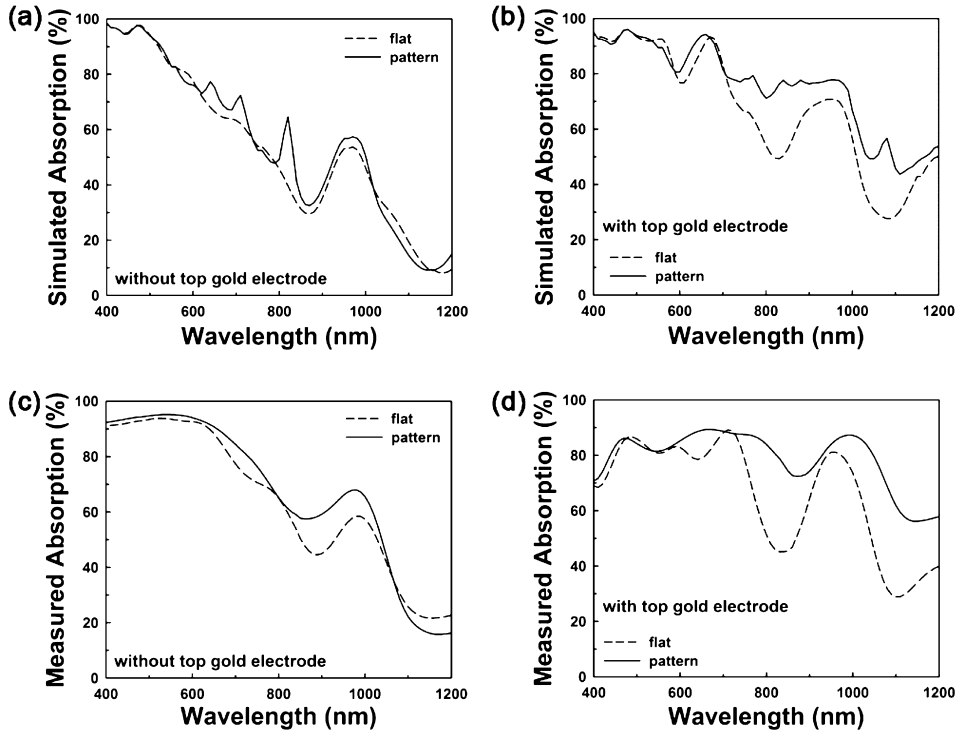

Figure 3. Simulated total absorption by FDTD simulations in flat and nanostructured solar cell devices (a) without top gold electrode and (b) with top gold electrode. Measured total absorption by UV−vis-IR spectroscopy in each flat and nanostructured solar cell devices (c) without top metal electrode and (d) with top metal electrode.

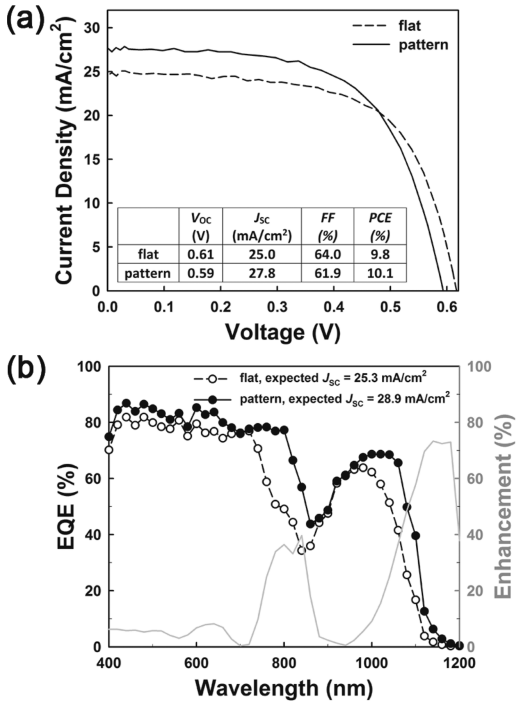

	V_{OC} (V)	J_{SC} (mA/cm²)	FF (%)	PCE (%)
flat	0.61	25.0	64.0	9.8
pattern	0.59	27.8	61.9	10.1

Figure 4. (a) Current density−voltage (J−V) curves of flat and nanostructured solar cell devices. (b) External quantum efficiency (EQE) curves of the flat and nanostructured solar cell devices. Gray solid line indicates the degree of EQE enhancement of the nanostructured device as a function of wavelength compared to flat device.

EQE in the wavelength regions in which the light absorption is insufficient in the flat device.

Nanostructured CQD-only films with the round-shaped motifs were produced using the NTP process, wherein CQDs are spin-coated onto a patterned PDMS mold and subsequently transferred to target substrates. These resulting CQD films enabled light trapping at the nanostructured back interface of bottom-illuminated solar cells to improve optical absorption and device performance. FDTD simulations support that light trapping in this device is enhanced using nanostructured CQD films. We obtained the improved J_{SC} (27.8 mA/cm^2) and PCE (10.1%) values as a result of the nanostructured back interface in CQD solar cells. The NTP process for nanostructuring CQD solids demonstrated here can be further utilized in various optoelectronic devices based on a number of solution-processed optoelectronic materials that incorporate CQDs, including photovoltaics and light-emitting diodes, to enhance device performance optically.

■ ASSOCIATED CONTENT

Supporting Information

The Supporting Information is available free of charge on the ACS Publications website at DOI: 10.1021/acs.nanolett.6b05241.

Detail experimental section and additional data (PDF)

■ AUTHOR INFORMATION

Corresponding Author

*E-mail: ted.sargent@utoronto.ca.

ORCID

Younghoon Kim: 0000-0003-0860-2156

Kristopher Bicanic: 0000-0002-3020-4093

Olivier Ouellette: 0000-0001-5708-5058

Author Contributions

The manuscript was written through contributions of all authors. All authors have given approval to the final version of the manuscript.

DOI: 10.1021/acs.nanolett.6b05241
Nano Lett. XXXX, XXX, XXX−XXX

Notes

The authors declare no competing financial interest.

■ ACKNOWLEDGMENTS

This publication was based in part on work supported by Award KUS-11-009-21, made by King Abdullah University of Science and Technology (KAUST), by the Ontario Research Fund - Research Excellence Program, and by the Natural Sciences and Engineering Research Council (NSERC) of Canada. H.T. acknowledges The Netherlands Organisation for Scientific Research (NWO) for a Rubicon Grant (680-50-1511) to support his postdoctoral research at University of Toronto. This work was also carried out under Qatar National Research Fund (QNRF) project NPRP-8-086-1-017. The authors thank L. Levina, R. Wolowiec, D. Kopilovic, and E. Palmiano for their technical help over the course of this research. O.O. received financial support from the Fonds de Recherche du Québec – Nature et Technologies (FRQNT).

■ REFERENCES

(1) Hines, M. A.; Scholes, G. D. *Adv. Mater.* **2003**, *15*, 1844−1849.
(2) McDonald, S. A.; Konstantatos, G.; Zhang, S.; Cyr, P. W.; Klem, E. J. D.; Levina, L.; Sargent, E. H. *Nat. Mater.* **2005**, *4*, 138−142.
(3) Gur, I.; Fromer, N. A.; Geier, M. L.; Alivisatos, A. P. *Science* **2005**, *310*, 462−465.
(4) Chuang, C.-H. M.; Brown, P. R.; Bulović, V.; Bawendi, M. G. *Nat. Mater.* **2014**, *13*, 796−801.
(5) Colvin, V. L.; Schlamp, M. C.; Alivisatos, A. P. *Nature* **1994**, *370*, 354−357.
(6) Sun, Q. J.; Wang, Y. A.; Li, L. S.; Wang, D. Y.; Zhu, T.; Yang, C. H.; Li, Y. F. *Nat. Photonics* **2007**, *1*, 717−722.
(7) Mashford, B. S.; Stevenson, M.; Popovic, Z.; Hamilton, C.; Zhou, Z.; Breen, C.; Steckel, J.; Bulović, V.; Bawendi, M.; Coe-Sullivan, S.; Kazlas, P. T. *Nat. Photonics* **2013**, *7*, 407−412.
(8) Bae, W. K.; Lim, J.; Lee, D.; Park, M.; Lee, H.; Kwak, J.; Char, K.; Lee, C.; Lee, S. *Adv. Mater.* **2014**, *26*, 6387−6393.
(9) Ip, A. H.; Thon, S. M.; Hoogland, S.; Voznyy, O.; Zhitomirsky, D.; Debnath, R.; Levina, L.; Rollny, L. R.; Carey, G. H.; Fischer, A.; Kemp, K. W.; Kramer, I. J.; Ning, Z.; Labelle, A. J.; Chou, K. W.; Amassian, A.; Sargent, E. H. *Nat. Nanotechnol.* **2012**, *7*, 577−582.
(10) Rath, A. K.; Bernechea, M.; Martinez, L.; García de Arquer, F. P.; Osmond, J.; Konstantatos, G. *Nat. Photonics* **2012**, *6*, 529−534.
(11) Kramer, I. J.; Zhitomirsky, D.; Bass, J. D.; Rice, P. M.; Topuria, T.; Krupp, L.; Thon, S. M.; Ip, A. H.; Debnath, R.; Kim, H.-C.; Sargent, E. H. *Adv. Mater.* **2012**, *24*, 2315−2319.
(12) Ning, Z.; Voznyy, O.; Pan, J.; Hoogland, S.; Adinolfi, V.; Xu, J.; Li, M.; Kirmani, A. R.; Sun, J.; Minor, J.; Kemp, K. W.; Dong, H.; Rollny, L.; Labelle, A.; Carey, G.; Sutherland, B. R.; Hill, I.; Amassian, A.; Liu, H.; Tang, J.; Bakr, O. M.; Sargent, E. H. *Nat. Mater.* **2014**, *13*, 822−828.
(13) Crisp, R. W.; Kroupa, D. M.; Marshall, A. R.; Miller, E. M.; Zhang, J.; Beard, M. C.; Luther, J. M. *Sci. Rep.* **2015**, *5*, 9945.
(14) Lan, X.; Voznyy, O.; Kiani, A.; García de Arquer, F. P.; Abbas, A. S.; Kim, G. H.; Liu, M.; Yang, Z.; Walters, G.; Xu, J.; Yuan, M.; Ning, Z.; Fan, F.; Kanjanaboos, P.; Kramer, I. J.; Zhitomirsky, D.; Lee, P.; Perelgut, A.; Hoogland, S.; Sargent, E. H. *Adv. Mater.* **2016**, *28*, 299−304.
(15) National Renewable Energy Labs (NREL) Efficiency Chart 2016. http://www.nrel.gov/pv/assets/images/efficiency_chart.jpg (accessed Aug. 2016).
(16) Liu, M.; Voznyy, O.; Sabatini, R.; García de Arquer, F. P.; Munir, R.; Balawi, A. H.; Lan, X.; Fan, F.; Walters, G.; Kirmani, A. R.; Hoogland, S.; Laquai, F.; Amassian, A.; Sargent, E. H. *Nat. Mater.* **2016**, *16*, 258−263.
(17) Clifford, J. P.; Konstantatos, G.; Johnston, K. W.; Hoogland, S.; Levina, L.; Sargent, E. H. *Nat. Nanotechnol.* **2009**, *4*, 40−44.
(18) Guyot-Sionnest, P. *J. Phys. Chem. Lett.* **2012**, *3*, 1169−1175.
(19) Tress, W.; Corvers, S.; Leo, K.; Riede, M. *Adv. Energy Mater.* **2013**, *3*, 873−880.
(20) Paz-Soldan, D.; Lee, A.; Thon, S. M.; Adachi, M. M.; Dong, H.; Maraghechi, P.; Yuan, M.; Labelle, A. J.; Hoogland, S.; Liu, K.; Kumacheva, E.; Sargent, E. H. *Nano Lett.* **2013**, *13*, 1502−1508.
(21) Zhou, L.; Yu, X.; Zhu, J. *Nano Lett.* **2014**, *14*, 1093−1098.
(22) Baek, S.-W.; Song, J. H.; Choi, W.; Song, H.; Jeong, S.; Lee, J.-Y. *Adv. Mater.* **2015**, *27*, 8102−8108.
(23) Tang, M.; Zhou, L.; Gu, S.; Zhu, W.; Wang, Y.; Xu, J.; Deng, Z.; Yu, T.; Lu, Z.; Zhu, J. *Appl. Phys. Lett.* **2016**, *109*, 183901.
(24) Kawawaki, T.; Wang, H.; Kubo, T.; Saito, K.; Nakazaki, J.; Segawa, H.; Tatsuma, T. *ACS Nano* **2015**, *9*, 4165−4172.
(25) Zhu, J.; Hsu, C.−M.; Yu, Z.; Fan, S.; Cui, Y. *Nano Lett.* **2010**, *10*, 1979−1984.
(26) Adachi, M. M.; Labelle, A. J.; Thon, S. M.; Lan, X.; Hoogland, S.; Sargent, E. H. *Sci. Rep.* **2013**, *3*, 2928.
(27) Mihi, A.; Beck, F. J.; Lasanta, T.; Rath, A. K.; Konstantatos, G. *Adv. Mater.* **2014**, *26*, 443−448.
(28) Labelle, A. J.; Thon, S. M.; Masala, S.; Adachi, M. M.; Dong, H.; Farahani, M.; Ip, A. H.; Fratalocchi, A.; Sargent, E. H. *Nano Lett.* **2015**, *15*, 1101−1108.
(29) Labelle, A. J.; Thon, S. M.; Kim, J. Y.; Lan, X.; Zhitomirsky, D.; Kemp, K. W.; Sargent, E. H. *ACS Nano* **2015**, *9*, 5447−5453.
(30) Leung, S.-F.; Zhang, Q.; Tavakoli, M. M.; He, J.; Mo, X.; Fan, Z. *Small* **2016**, *12*, 2536−2548.
(31) Ferry, V. E.; Polman, A.; Atwater, H. A. *ACS Nano* **2011**, *5*, 10055−10064.
(32) Deceglie, M. G.; Ferry, V. E.; Alivisatos, A. P.; Atwater, H. A. *Nano Lett.* **2012**, *12*, 2894−2900.
(33) Yan, B.; Yue, G.; Sivec, L.; Owens-Mawson, J.; Yang, J.; Guha, S. *Sol. Energy Mater. Sol. Cells* **2012**, *104*, 13−17.
(34) Sai, H.; Saito, K.; Kondo, M. *Appl. Phys. Lett.* **2012**, *101*, 173901.
(35) Lee, Y. H.; Lee, T. K.; Song, I.; Yu, H.; Lee, J.; Ko, H.; Kwak, S. K.; Oh, J. H. *Adv. Mater.* **2016**, *28*, 4976−4982.
(36) Mihi, A.; Bernechea, M.; Kufer, D.; Konstantatos, G. *Adv. Opt. Mater.* **2013**, *1*, 139−143.
(37) Park, C.; Lee, T.; Xia, Y.; Shin, T. J.; Myoung, J.; Jeong, U. *Adv. Mater.* **2014**, *26*, 4633−4638.
(38) Jang, D.; Kim, Y.; Kim, T. Y.; Koh, K.; Jeong, U.; Cho, J. *Nano Energy* **2016**, *20*, 283−293.
(39) Yu, K. J.; Gao, L.; Park, J. S.; Lee, Y. R.; Corcoran, C. J.; Nuzzo, R. G.; Chanda, D.; Rogers, J. A. *Adv. Energy Mater.* **2013**, *3*, 1401−1406.
(40) Tan, H.; Furlan, A.; Li, W.; Arapov, K.; Santbergen, R.; Wienk, M. M.; Zeman, M.; Smets, A. H.; Janssen, R. A. J. *Adv. Mater.* **2016**, *28*, 2170−2177.

DOI: 10.1021/acs.nanolett.6b05241
Nano Lett. XXXX, XXX, XXX−XXX